Supporting Information for

Quantitative Analysis of FAI-Diffusion in Sequentially Evaporated $FAPbI_3$ Perovskite Thin Films

Tobias Schulz[1], Matthias Maiberg[1], Marcel Schrader[1], Roland Scheer[1], Paul Pistor[2]

[1] Martin-Luther-University Halle-Wittenberg Von-Danckelmann-Platz 3, 06120 Halle (Saale), Germany

[2] Center for Nanoscience and Sustainable Technologies (CNATS), Department of Physical, Chemical, and Natural Systems, Universidad Pablo de Olavide (UPO), Carretera de Utrera 1, 41013 Sevilla, Spain

This Supporting Information (SI) provides additional data and discussions supporting the hypotheses and conclusions of the main text. It starts by showing colormaps of the in situ XRD measurements of all the deposition processes of the different isothermal annealing experiments presented in the main text, together with an exemplary description of the experiment with a nominal isothermal annealing temperature of 100°C. After that, the colormaps of the remaining annealing experiments are listed.

Next, we present and discuss the temperature correction and presence of the 2D FA_2PbI_4 phase, before providing SEM images of a non-annealed and annealed film. The Arrhenius plots for the initial PVK thickness $d_{PVK,0}$ and starting time t_0 variation are also depicted for comparison. Then, the FAI and PVK peak transient fitting results for all not already shown temperatures are displayed. The Supporting Information is concluded by three tables: the calculation of the saturation concentration, calculation of the relative Intensity I_{rel}, and the initial and fit parameters for all annealing temperatures.

The in situ diffractogram for the nominal 100°C experiment of the deposition is depicted in Fig S1. The upper graph shows the in situ diffractogram. In the graph below, the integrated intensity of chosen diffraction peaks is depicted. Also, the laser light scattering (LLS) signal and deposition rate is plotted. The shaded areas mark the times of PbI_2 (orange) and FAI (red) deposition, respectively. At the beginning, during the PbI_2 evaporation, a prominent peak arises at 12.7°, which represents the (001) orientation of the 2H polytype of the hexagonal PbI_2. The (002) peak at 25.5° is also visible with a low intensity. After reaching a maximum integrated intensity, its intensity decreases rapidly again, although PbI_2 is still deposited, which can be seen in the LLS data. This method can be used to estimate layer thickness as well as texture changes of the film via thin film interference. A detailed explanation of this method is given in previous reports(1). We use two different wavelengths, 650 nm (depicted in red) and 1550 nm (grey). The number of oscillations give information about the deposited film thickness. The continuous oscillations for both laser wavelengths verify, that PbI_2 indeed got deposited the whole time. However, it can be seen, that a new peak at 28.3° appears, which has a monotonous increasing integrated intensity. This peak does not match with any reference for the hexagonal 2H PbI_2 but fits the rhombohedral 6R polytype of PbI_2. In a previous report, we already investigated this

phenomena(2). This indicates, that first a 2H PbI_2 layer is growing and after reaching a critical thickness, the 6R polytype is preferred. This 6R layer acts as a source of x-ray attenuation for the underlying 2H layer. For the 2H (001) peak, the angle of incident ω and detector angle Ω are 12 and 0.7°, respectively. This geometry creates very large x-ray pathways, which causes significant attenuation effects. Because of that, the growing 6R layer attenuates the x-rays drastically, which contribute to the 2H (001) diffraction signal, leading to a detectable intensity decrease. At the end of the PbI_2 deposition, no clear 2H (001) is visible anymore, only the 2H (002) and 6R (104) at 28.3°. Upon FAI deposition a diffraction peak arises at 14°, which marks the formation of α-$FAPbI_3$. This reaction happens as soon as FAI is in contact with PbI_2, even at room temperature. At the same time the peak at 28.3° is also increasing in intensity, which is due to $FAPbI_3$ having its (200) peak at almost the same position and thus making a differentiation between (104) 6R PbI_2 and (200) $FAPbI_3$ not possible. After a small $FAPbI_3$ film growth, the intensity of PVK peaks is decreasing again, which can be explained by the formation of lower dimensional perovskites (LDP), which will be discussed in the next chapter and attenuation due to the growing FAI layer. Also, FAI diffraction peaks can be seen at 24.7 and 25.6°. As the (002) 2H PbI_2 layer is in superposition with the 25.6° () FAI peak, making in individual intensity evaluation of the (002) PbI_2 peak impossible. In conclusion, while we do verify the correct PbI_2 deposition via LLS, we cannot identify indistinguishably any PbI_2 diffraction peaks because of the used geometry used and the formation of the 6R polymorph. This is the reason we cannot use the decrease of individual PbI_2 peaks as a measure of PbI_2 consumption/perovskite formation, as we do for the FAI decrease, for example.

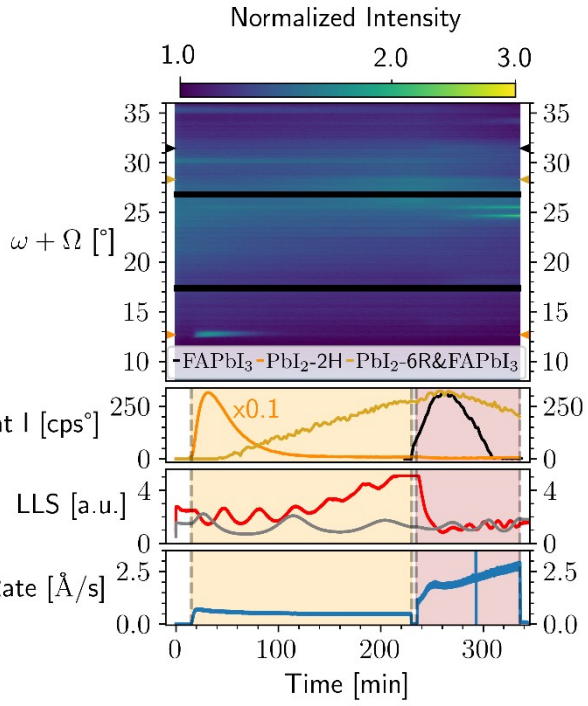

Figure S1 In situ diffractograms of the deposition step for the nominal 100°C annealing experiment. Besides the XRD data, also the integrated intensity of the $FAPbI_3$ (210) peak, the LLS, and the deposition rate are shown.

Determination of the initial PVK thickness $d_{PVK,0}$

The initial PVK layer is determined with the deposition in situ diffractogram seen in Figure S1. At the beginning of the FAI deposition, PVK peaks are appearing, for example the (210) orientation at 31.4° (3D). This indicates, that upon contact of FAI and PbI_2, the perovskite is formed, even at room temperature (25°C substrate temperature during deposition). With the maximum in integrated intensity for the 31.4° peak (316cps°) and the determined α (1.44 cps°/nm), the initial PVK thickness $d_{PVK,0}$ is calculated as 219 nm. Also seen is the laser light scattering (LLS) signal. This method can be used to estimate layer thickness as well as texture changes of the film. A detailed explanation of this method is given in previous reports(3). We use two different wavelengths, 650 nm (depicted in red) and 1550 nm (grey).

The number of oscillations give information about the deposited film thickness. It can be seen in Figure S1 (for nominal 100°C) as well as in Figure S2 (for all other temperatures), that in all experiments around 6 (2.5) oscillations are visible for the 650 nm (1550 nm) laser during the PbI_2 deposition, indicating an equal thickness in all experiments. The initial drop of the 650 nm laser intensity is due to a reduction in surface roughness. After that intensity decay around 5.5 and 2.5 oscillations are detectable for each respective laser for all experiments, again verifying equal film thicknesses.

Remaining colormaps

For completeness, we present in the following the remaining diffractograms in colormap representation, for all deposition and annealing processes, i.e. the ones that are not already displayed in the main text.

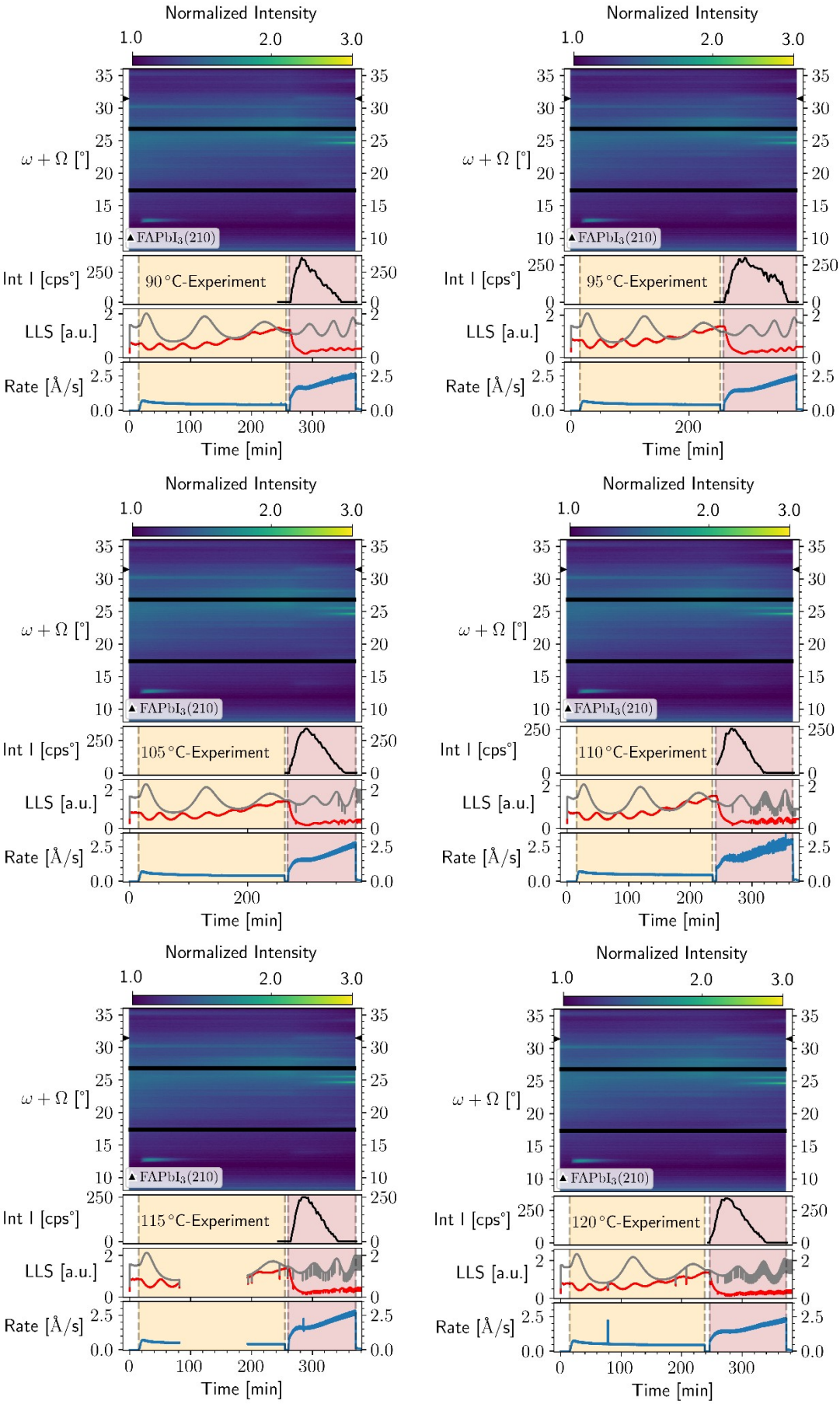

Figure S2 In situ diffractograms represented as colormaps of the deposition for the 90°C, 95°C, 105°C, 110°C, 115°C, and 120°C experiments. Besides the XRD data, also the integrated intensity of the $FAPbI_3$ (210) peak, the LLS, and the deposition rate are shown.

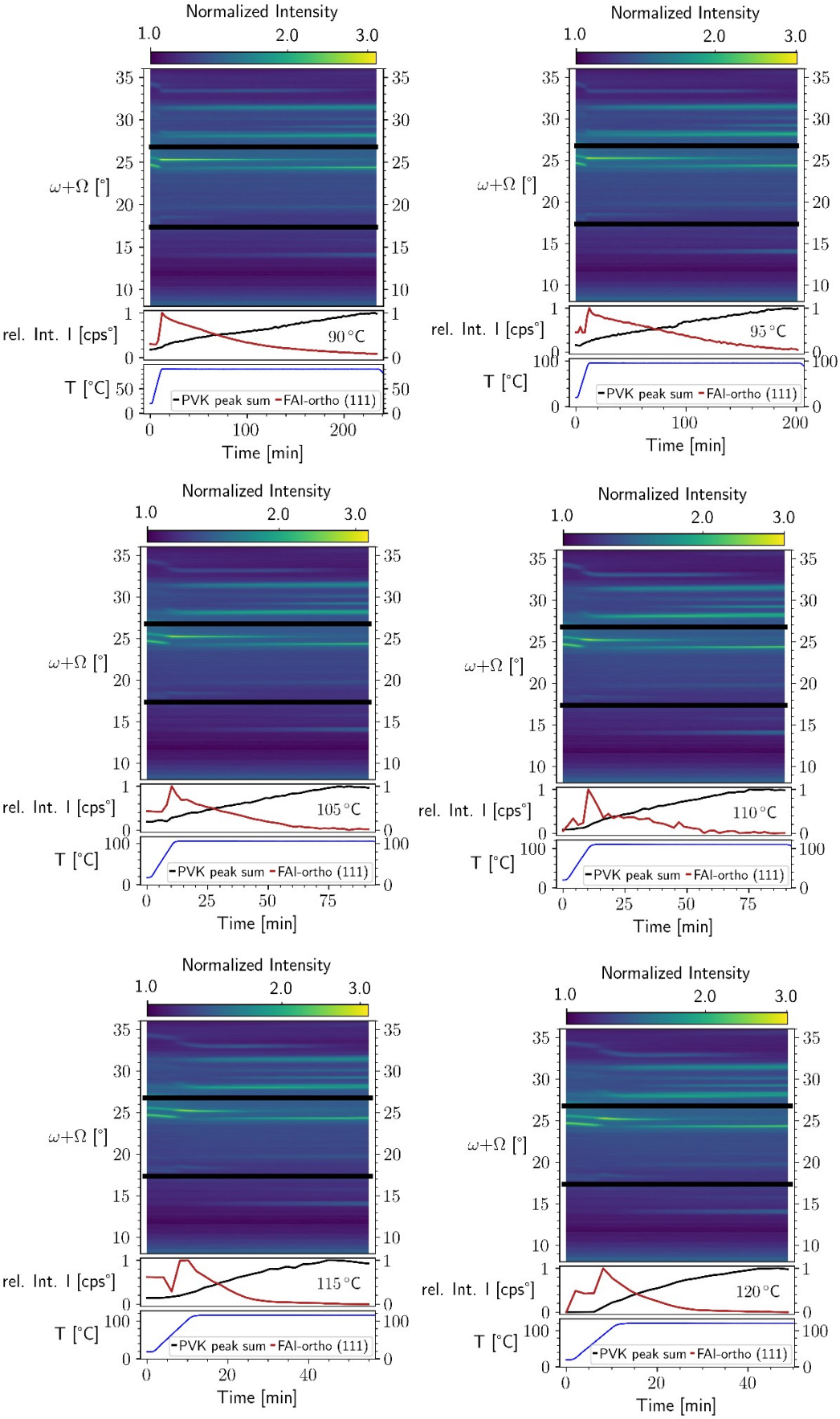

Figure S3 In situ diffractograms represented as colormaps for the 90°C, 95°C, 105°C, 110°C, 115°C, and 120°C annealing experiments. Besides the XRD data, also the integrated intensity of the PVK peak sum and the orthorhombic FAI (111) peak, as well as the nominal substrate temperature are shown.

Temperature Correction

The substrates are heating with infrared radiation from the back, and therefore a temperature gradient towards the front side of the 1.1 mm thick glass substrate is formed. To estimate the difference between the temperature at the front and back side of the samples, we heat the samples with the nominal annealing temperature (applied and measured at the back side) and measured the front side temperature using self-adhesive temperature labels. The results can be seen in Figure S4. The separated areas on the labels are turning black, when the corresponding temperature is reached. As see, they can label the temperature in 5-6°C steps. Because we do not know the exact temperature, we assume that the front side reached a temperature in the middle between the last black and first white area. For example, the left substrate in Figure S4 (Nominal temperature 121°C): Here, 99°C are reached at the front side of the sample, but also temperatures up to 103°C are possible, without changing the result of the label. Because of that, we assume the front side to have reached a temperature between 104°C and 99°C, namely 101.5°C. This creates a difference to the set back side temperature of 19.5°C. Averaging over all labels, we get a difference between back and front side of around 16°C.

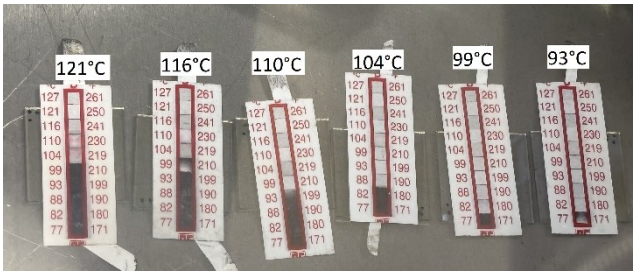

Figure S4 Photograph of the used temperature labels. The black color indicates, that the corresponding temperature got reached at the front side of the samples. The temperatures above are the nominal back side temperatures.

Due to the difficult temperature reading inside a vacuum chamber, we assume a temperature uncertainty of maximum 10°C. Figure S5 shows three Arrhenius plots, where the effect upon the diffusion parameters can be seen. The blue graph represents Figure 8 from the main manuscript without consideration of uncertainties due to c_s, $d_{PVK,0}$, and t_0. By reducing all temperatures by 10°C (orange) or increasing by 10°C (green) a minor deviation for the activation energy of 0.04-0.05 eV is observable. The preexponential factor does change by a factor of 2. These results indicate, that the error due to the temperature reading uncertainty is on the same scale as all the other mentioned uncertainty sources.

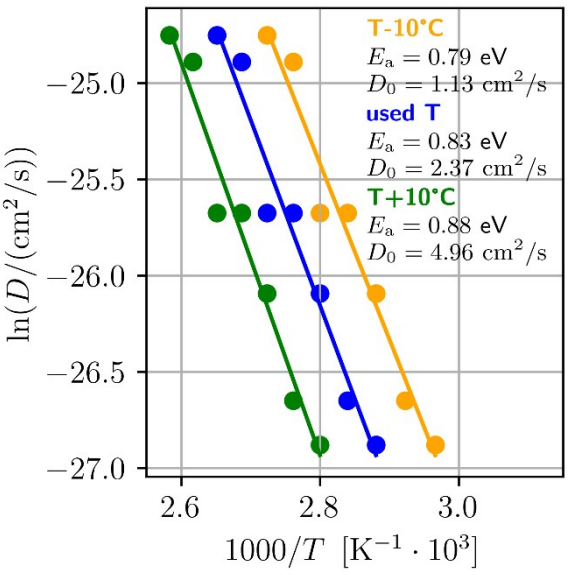

Figure S5 Arrhenius plots to analyse temperature uncertainties and its effect on the diffusion parameters. By assuming a 10°C uncertainty, the estimated activation energy does change by 0.04-0.05 eV. For the preexponential factor a factor of 2 difference can be seen. For visibility reasons error bars are not shown.

Peak labelling

Figure S6 shows the in situ diffractogram for the nominal 100°C annealing temperature experiment. All intense and relevant peaks for this publication are highlighted with a colored triangle. An extract of the diffractogram at 89 min. is displayed in Figure S7. Here, the existence of the 2D phase is clearly visible. However, the relatively small intensity and the FAI peak in close vicinity make a precise evaluation not possible.

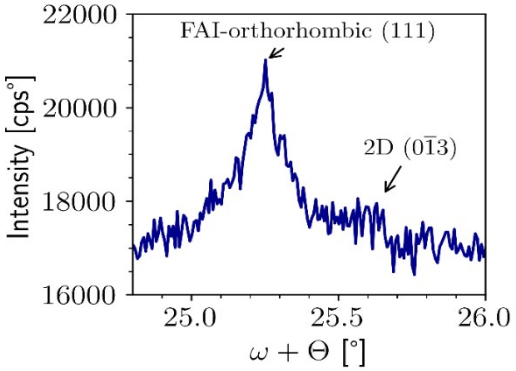

Figure S7 Extract of the diffractogram of the 100°C annealing experiment taken at 89 min. Both, the intense FAI and the small 2D PVK peak are visible, indicating the presence of the 2D phase.

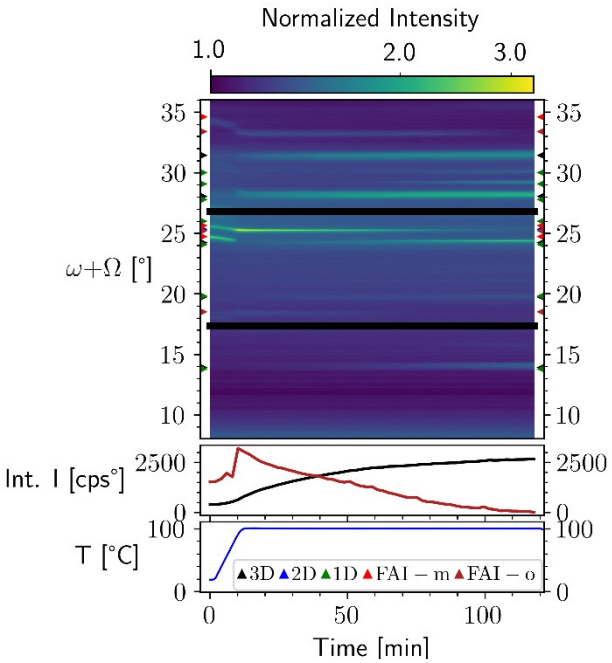

Figure S6 In situ diffractograms of the nominal 100°C annealing experiment with reference peak positions for all detectable PVK phases as well as monoclinic and orthorhombic FAI.

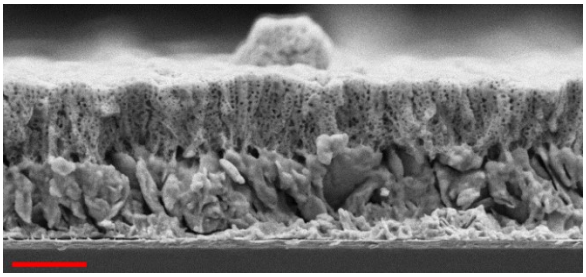

Figure S8 SEM image of non-annealed PbI2 (645nm) and FAI (1200nm) film. Scale bar is 1µm.

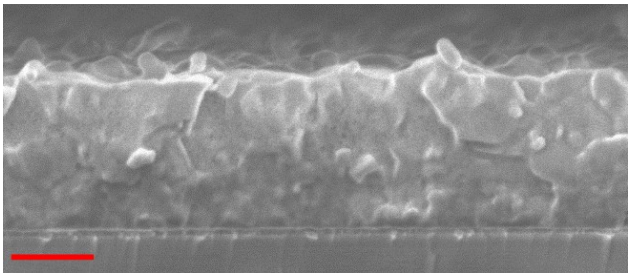

Figure S9 SEM image of the 100°C experiment. The average film thickness is estimated as 1.85 µm. Scale bar is 1µm.

SEM images

Figure S8 shows the SEM image of a 645 nm PbI_2 and 1200 nm FAI layer, which was not annealed. Both layers are clearly distinguishable, which supports our initial assumption of a one-dimensional diffusion. In Figure S9 the SEM image of the nominal 100°C experiment is displayed. Here, a homogenous film is seen. The average thickness is around 1850 nm.

Attenuation Consideration

To estimate the effect of x-ray attenuation the following experiment was conducted: FAI and PbI_2 were co-evaporated on an ITO/PTAA substrate. With an x-ray angle of incident ω=12° the PVK peak at 24° was measured, the result can be seen in Figure S10. The integrated intensity grows almost linearly until a thickness of around 2µm. After that the typical $1 - exp(-\mu * s)$ shape is visible. Here µ is the linear attenuation coefficient and $s = \frac{2d}{sin(\theta)}$ the x-ray path inside the sample with $\omega = \Omega = \theta = 12°$. The linearity up to 2µm means, that up to this thickness, attenuation effects do not have a significant impact on the measured X-ray intensities, and can therefore be neglected in our experiments. Additionally, this graph verifies our assumption of a constant $\alpha = \frac{I}{d}$ value, which is the slope in Figure S10.

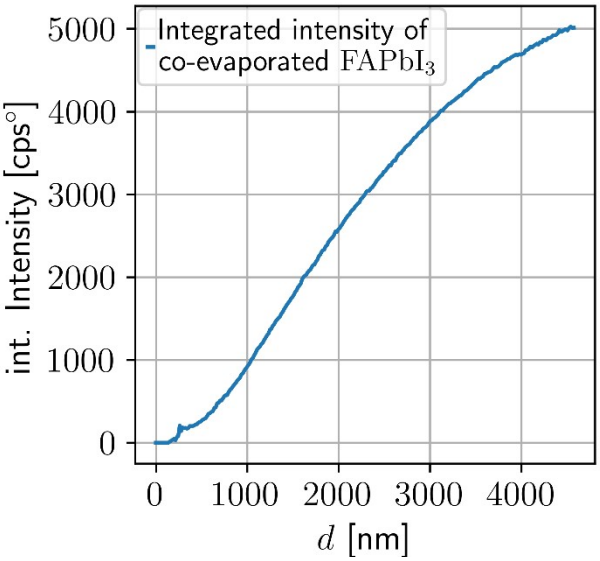

Figure S10 Integrated intensity of the 24° PVK peak (ω=12°) in dependency of deposited $FAPbI_3$ via co-evaporation.

Effect of different PVK starting thickness $d_{PVK,0}$

Figure S11 shows the Arrhenius plot for different starting PVK thicknesses $d_{PVK,0}$ with c_s/c_0=80%. In blue the already shown data points and fit from Figure 8 of the main script are displayed for comparison. Additionally, the resulting temperature dependent diffusion coefficients for $d_{PVK,0}$=100 nm (orange) and 500 nm (green) are given. It can be seen, that choosing a smaller starting thickness results in no significant change in the activation energy and preexponential factor. By increasing the starting thickness, the activation energy and preexponential factor increase by 0.05 eV and 8.82 cm^2/s, respectively. Nevertheless, the impact of a different starting thickness remains rather small.

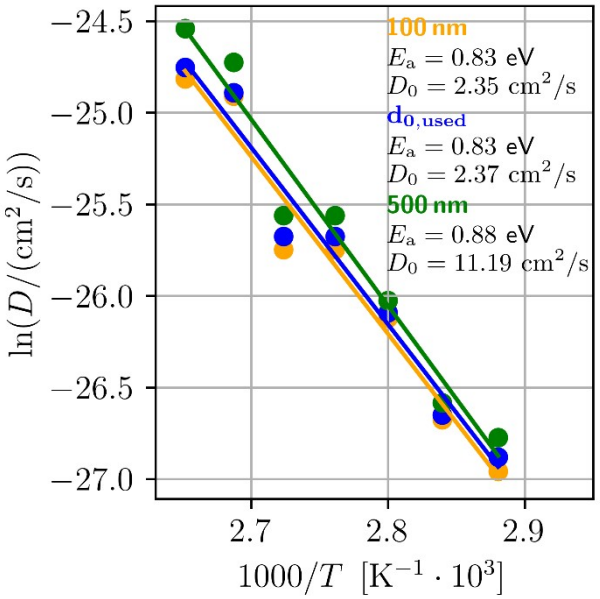

Figure S11 Arrhenius Plot for the used starting thickness d_0 written in Table 3 (blue) as well as 100 nm (orange) and 500 nm (green). For c_s/c_0 80% was chosen.

Effect of different starting times t_0

When the starting time (first data point to be considered in the fitting) is varied from 10 min. (reference value) to 12 min. only a minor difference in the activation energy (0.04 eV) and a factor of 4 in the preexponential factor is observed, as can be seen in Figure S12. A larger discrepancy is visible when comparing 8 min. This can be explained by the fact, that possibly the phase transition from the monoclinic to the orthorhombic FAI phase has not been completed. As seen in Figure 7 and S13, the orthorhombic FAI peak intensity did not reach its maximum value after 8 minutes, leading to a large fitting error and thus increases the diffusion coefficient uncertainty. This is especially crucial for the high temperature experiments, because there less measurement points exists, which increases the absolute error, according to Equation (15) in the main text.

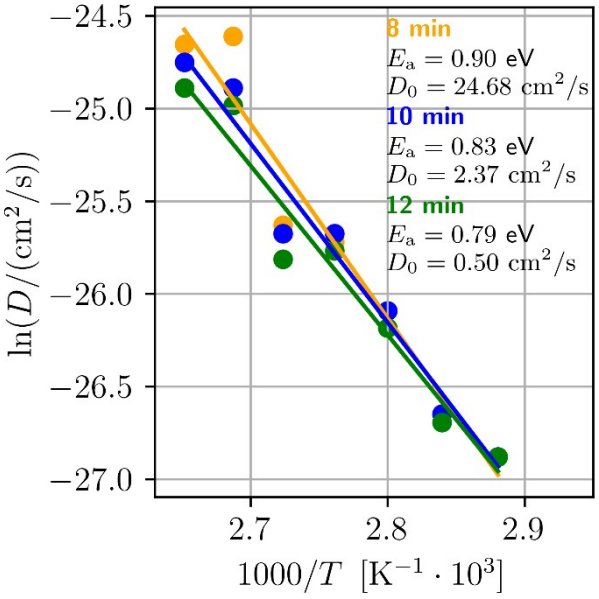

Figure S12 Arrhenius Plot for the used starting time t_0 (10 min, blue) as well as 8 min (orange) and 12 min (green). For c_s/c_0 80% was chosen.

Fit Plots for 90, 95, 105, 110, 115, and 120°C nominal annealing temperature experiments

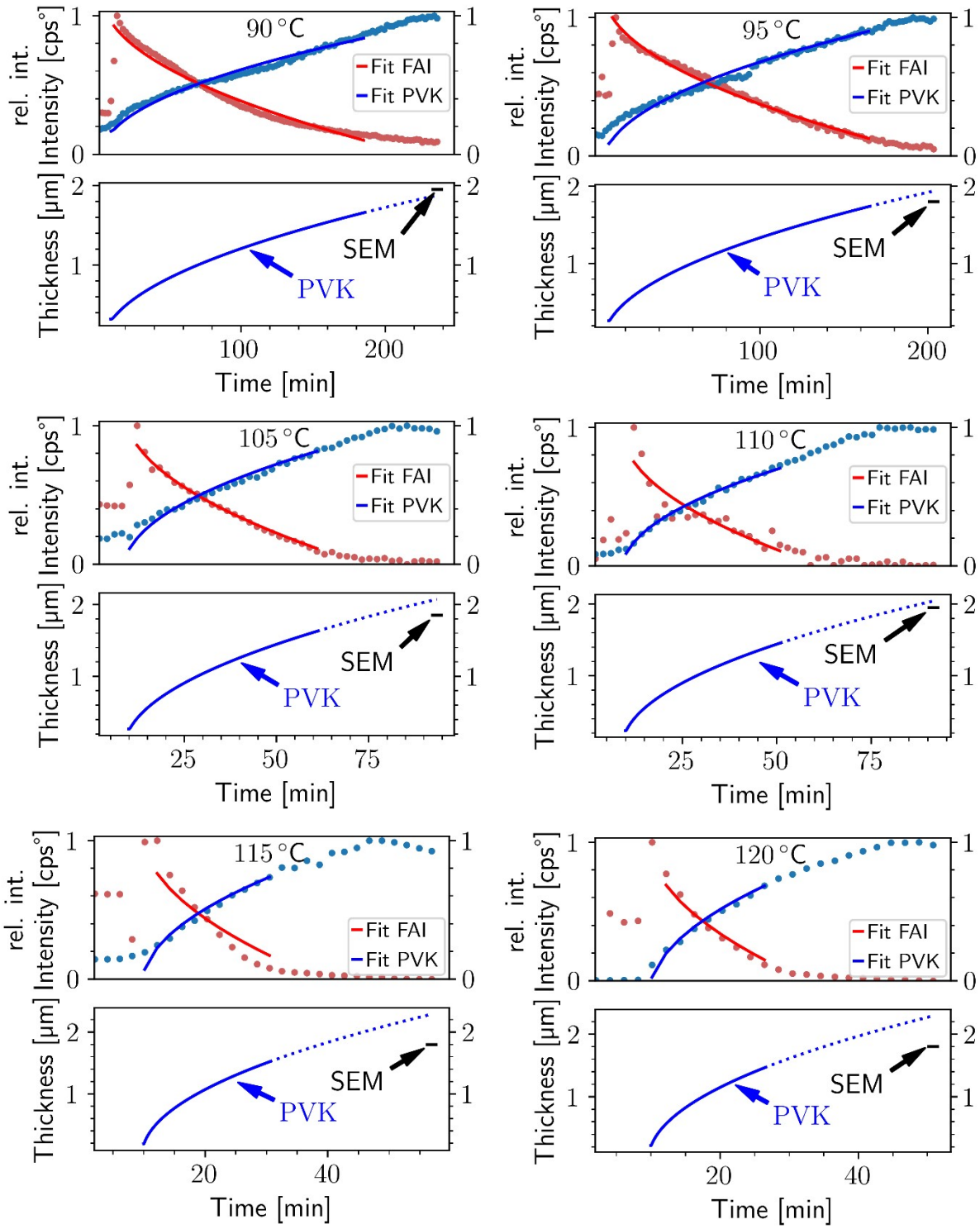

Figure S13 Normalised measured data as well as simulated intensities for the FAI (111) peak and the weighted sum of all detectable PVK signals (top) and time depended thickness of PVK layer (bottom) for shown nominal annealing temperatures.

Table for calculating the saturation concentration

Table S1 MAI and FAI concentration values to estimate the saturation concentration. c_s/c_0 gives the MAI or FAI concentration in the different dimensional perovskites referenced to pure MAI or FAI, respectively. Please note that for the regular 1D and 0D FAPI phases, no reference values for crystal structure parameters were found in literature.

Perovskite	Dimensionality and space group	V_{UC} [Å^3]	MAI/FAI particle number	MAI/FAI Concentration [mmol/cm^3]	c_s / c_0 [%]	Reference
$MAPbI_3$	3D (P1)	486.27	2	6.83	48.5	(4)
MA_2PbI_4	2D (P1)	724.88	4	9.16	65.1	(4)
MA_3PbI_5	1D (P1)	939.22	6	10.61	73.3	(4)
MA_4PbI_6	0D (P1)	599.45	4	11.08	78.7	(4)
$FAPbI_3$	3D ($Pm\bar{3}m$)	257.0	1	6.46	45.0	(5)
FA_2PbI_4	2D (P1)	329.5	2	10.08	70.2	(6)

Parameters to calculate the relative intensity I_{rel}

Table S2 Table to calculate I_{rel}. Besides the peak position 2θ, the dimension of the phase, structure amplitude |F|, multiplicity MU, product of angular dependent geometry and polarisation factor G*P, and the final relative intensity I_{rel} are given. Additionally, the XRD-reference is given in the last column. Please note that for the regular 1D and 0D FAPI phases, no reference values for crystal structure parameters were found in literature. The 1D FAPI phase mentioned here refers to a 1D $(iFA)_3PbI_5$ phase listed in reference *(7)*, which matches the peak positions of our experiments.

ω+Ω [°]	Dimension	|F|	MU	G*P	I_{rel}	Reference
13.8	1D	730.39	2	299.04	$3.19*10^8$	(7)
13.9	3D	124.21	6	279.10	$2.58*10^7$	(5)
19.7	3D	33.34	12	67.42	$8.99*10^5$	(5)
24.1	1D	648.14	2	42.16	$3.65*10^7$	(7)
24.2	3D	69.74	8	41.60	$1.61*10^6$	(5)
27.8	1D	892.24	2	31.52	$5.02*10^7$	(7)
28.0	3D	212.81	6	30.95	$8.41*10^6$	(5)
29.1	1D	672.74	4	28.89	$5.23*10^7$	(7)
30.0	1D	669.57	4	27.23	$4.88*10^7$	(7)
31.4	3D	111.49	24	24.98	$7.45*10^6$	(5)

Table with initial and fit parameters

Table S3 In this table all initial parameters are given as well as the resulting diffusion coefficient *D* for c_s/c_0 of 70 and 80%.

Exp.	$d_{PVK,0}$ [nm]	d_{SEM} [nm]	α [cps°/m]	t_{end} [min] 70% / 80%	D [cm^2/s] (70%)	D [cm^2/s] (80%)
90°C	322	1950	529.9	195 / 185	$3.07*10^{-12}$	$2.12*10^{-12}$
95°C	262	1800	640.2	173 / 165	$3.70*10^{-12}$	$2.67*10^{-12}$
100°C	219	1850	699.5	89.5 / 87.4	$6.15*10^{-12}$	$4.66*10^{-12}$
105°C	267	1850	649.4	61 / 61	$9.33*10^{-12}$	$7.07*10^{-12}$
110°C	233	1950	626.3	50.8 / 50.8	$9.33*10^{-12}$	$7.07*10^{-12}$
115°C	187	1800	689.2	30.5 / 30.5	$1.96*10^{-11}$	$1.55*10^{-11}$
120°C	219	1800	753.8	28.5 / 26.4	$2.47*10^{-11}$	$1.78*10^{-11}$

Table for literature comparison

Although our activation energy of 0.84 eV is comparable with literature, calculated diffusion coefficients might differ. To understand that discrepancy, table S4 was generated, which shows diffusion parameters for different ions from various publications. Each publication only stated the activation energies for the diffusing ions and diffusion coefficients at one single temperature. These values were taken to calculate the preexponential factor and the diffusion coefficient at 105°C. As seen in the table, the iodine ion is moving faster, than the A-cation counterpart. Additionally, huge deviations between the diffusion coefficients at 105°C for the MA^+ particles can be seen. Within the same work, a two order of magnitude difference between the $MAPbI_3$ crystal structure is visible. Also, the measurement type influences the final result by multiple orders of magnitude. These results show on one hand, that the MA and FA systems give comparable results due to the chemically similarity and on the other hand, that the diffusion coefficients also depend on the used measurement devices. Our value for the diffusion coefficient at 105°C is located within the diffusion coefficient interval for the MA^+ diffusion through $MAPbI_3$.

Table S4 Collection of Arrhenius parameters and diffusion coefficients (at 105°C) from selected literature reports. For all stated publications the preexponential factor D_0 was calculated by given diffusion coefficients at other temperatures.

Ion	Measurement	E_a [eV]	D_0 [cm^2/s]	D(105°C) [cm^2/s]	Reference
I^-	Theoretical calculation	0.58	$1.4*10^{-3}$	$2.6*10^{-11}$	(8)
MA^+ (cubic)		0.84	$1.7*10^{-3}$	$1.0*10^{-14}$	
I^-	Transient ion-drift measurements	0.29	$2.3*10^{-4}$	$3.1*10^{-8}$	(9)
MA^+ (tetragonal)		0.9	$4.5*10^{+3}$	$4.7*10^{-9}$	
MA^+ (cubic)		0.39	$5.7*10^{-6}$	$3.6*10^{-11}$	
MA^+ (cubic)	NRM tracer self diffusion			$(0.9\text{-}6)*10^{-13}$	(10)
FAI	Concentration driven diffusion measured via XRD	0.84±0.18	$1.2*10^{-2}$-$1.1*10^{+3}$	$7.07*10^{-12}$	This work

References

1. Hartnauer S, Wägele LA, Syrowatka F, Kaune G, Scheer R. Co-evaporation process study of Cu2ZnSnSe4 thin films by in situ light scattering and in situ X-ray diffraction. Phys Status Solidi A. 2015;212(2):356–63. doi:10.1002/pssa.201431497

2. Heinze KL, Schulz T, Scheer R, Pistor P. Structural Evolution of Sequentially Evaporated (Cs,FA)Pb(I,Br)3 Perovskite Thin Films via In Situ X-Ray Diffraction. Phys Status Solidi A. 221(3):2300690. doi:10.1002/pssa.202300690

3. Scheer R, Pérez-Rodríguez A, Metzger WK. Advanced diagnostic and control methods of processes and layers in CIGS solar cells and modules. Prog Photovolt Res Appl. 2010;18(6):467–80. doi:10.1002/pip.966

4. Yokoyama T, Ohuchi S, Igaki E, Matsui T, Kaneko Y, Sasagawa T. An Efficient ab Initio Scheme for Discovering Organic–Inorganic Hybrid Materials by Using Genetic Algorithms. J Phys Chem Lett. 2021 Mar 4;12(8):2023–8. doi:10.1021/acs.jpclett.1c00087

5. Fabini DH, Stoumpos CC, Laurita G, Kaltzoglou A, Kontos AG, Falaras P, et al. Reentrant Structural and Optical Properties and Large Positive Thermal Expansion in Perovskite Formamidinium Lead Iodide. Angew Chem Int Ed. 2016;55(49):15392–6. doi:10.1002/anie.201609538

6. Fraccarollo A, Cantatore V, Boschetto G, Marchese L, Cossi M. Ab initio modeling of 2D layered organohalide lead perovskites. J Chem Phys. 2016 Apr 28;144(16):164701. doi:10.1063/1.4947305 PubMed PMID: 27131557.

7. Wang S, Mitzi DB, Feild CA, Guloy A. Synthesis and Characterization of [NH2C(I):NH2]3MI5 (M = Sn, Pb): Stereochemical Activity in Divalent Tin and Lead Halides Containing Single .ltbbrac.110.rtbbrac. Perovskite Sheets. J Am Chem Soc. 1995 May 1;117(19):5297–302. doi:10.1021/ja00124a012

8. Eames C, Frost JM, Barnes PRF, O'Regan BC, Walsh A, Islam MS. Ionic transport in hybrid lead iodide perovskite solar cells. Nat Commun. 2015 Jun 24;6(1):1. doi:10.1038/ncomms8497

9. Futscher MH, Lee JM, McGovern L, Muscarella LA, Wang T, Haider MI, et al. Quantification of ion migration in CH3NH3PbI3 perovskite solar cells by transient capacitance measurements. Mater Horiz. 2019 Aug 12;6(7):1497–503. doi:10.1039/C9MH00445A

10. Senocrate A, Moudrakovski I, Acartürk T, Merkle R, Kim GY, Starke U, et al. Slow CH3NH3+ Diffusion in CH3NH3PbI3 under Light Measured by Solid-State NMR and Tracer Diffusion. J Phys Chem C. 2018 Sep 27;122(38):21803–6. doi:10.1021/acs.jpcc.8b06814